Test of the Dynamic-Domain and Critical Scattering Hypotheses in Cubic Methylammonium Lead Triiodide

Nicholas J. Weadock,[1] Peter M. Gehring,[2] Aryeh Gold-Parker,[3] Ian C. Smith,[3] Hemamala I. Karunadasa,[3,4] and Michael F. Toney[1,*]

[1]SSRL Materials Science Division, SLAC National Accelerator Laboratory, Menlo Park, California 94025, USA
[2]NIST Center for Neutron Research, National Institute of Standards and Technology, Gaithersburg, Maryland 20899, USA
[3]Department of Chemistry, Stanford University, Stanford, California 94305, USA
[4]Stanford Institute for Materials and Energy Sciences, SLAC National Accelerator Laboratory, Menlo Park, California 94025, USA

(Received 18 May 2020; accepted 7 July 2020; published 10 August 2020)

We investigate the hypothesis of dynamic tetragonal domains occurring in cubic $CH_3NH_3PbI_3$ using high-resolution neutron spectroscopy to study a fully deuterated single crystal. The R-point scattering above the 327.5 K cubic-tetragonal phase transition is always resolution limited in energy and therefore inconsistent with dynamic-domain predictions. This behavior is instead consistent with the central peak phenomenon observed in other perovskites. The scattering may originate from small, static, tetragonal-phase domains nucleating about crystal defects, and the temperature dependence demonstrates the transition is first order.

DOI: 10.1103/PhysRevLett.125.075701

Hybrid organic-inorganic metal-halide perovskites (HOIPs) are a novel class of semiconductor with unusual and promising optoelectronic properties for high-efficiency devices. The HOIP family exhibits significant dynamical disorder due to weak bonding and the rotational degrees of freedom of the organic cations [1,2]. This disorder is believed to affect optoelectronic and other properties [3–6]. Dynamical disorder also correlates with phase transitions in the prototypical HOIP, $CH_3NH_3PbI_3$ (herein MAPI), which transitions between orthorhombic, tetragonal, and cubic phases at 162 K and 327.5 K, respectively [7]. The cubic-tetragonal transition in MAPI proceeds as a condensation of the soft, transverse acoustic, cubic R-point phonon [4,8]. The cubic R point becomes the Γ point of the tetragonal phase, giving rise to elastic Bragg scattering [4,8,9]. X-ray inelastic scattering studies have observed R-point scattering in cubic MAPI, and analysis of x-ray pair-distribution functions (PDF) suggests domains of lower symmetry or dynamic off-centering exists for $r < 8$ Å in the cubic phase of HOIPs [4,8,10,11]. These reports have led to predictions of tetragonal domains within cubic MAPI that are both small and potentially dynamic [4,6,8]. Computational results at 650 K (above the experimentally observed decomposition temperature [12]) indicate sub-ps lifetimes for these domains [5]. In addition, the hypothesis of dynamic tetragonal domains has been used to explain the lack of variation in optoelectronic properties of MAPI-based devices between the two phases [9].

Materials that exhibit soft-mode-driven structural phase transitions often display diffuse "critical scattering" arising from structural fluctuations, like the postulated dynamic domains, near the critical temperature T_C [13]. Apparent critical behavior has been studied extensively with neutron and x-ray scattering methods in perovskite compounds, including $SrTiO_3$, $KMnF_3$, $RbCaF_3$, $CsPbCl_3$, $CsPbBr_3$, and $MAPbCl_3$ [14–25].

In these materials, neutron inelastic scattering experiments found certain soft-mode transitions that exhibit an anomalous central peak (CP) centered at $\hbar\omega = 0$. First reported in $SrTiO_3$ in 1971 by Riste *et al.* [26], the evidence to date indicates that the CP is resolution limited in energy and therefore a static (infinite lifetime) phenomenon; it thus differs from critical scattering, which is dynamic in nature. Several theories of the CP origin have been proposed [27]. Shapiro and coworkers demonstrated that anharmonic renormalization of the soft-mode phonon results in a scattering function consisting of phonon sidebands plus a central component centered at zero energy [15]. Other studies have proposed that the CP arises from domains of the low-temperature structure nucleating at defects [18,28,29]. A second, longer length scale has been observed in high-resolution x-ray and neutron scattering studies of critical scattering; however, this narrow component is unrelated to the CP because it is absent in the bulk and is due to static Bragg scattering from regions of the low-temperature phase nucleating near the sample surface [14,20,21,30–33].

We use high-resolution neutron spectroscopy, with an energy resolution at least 10 times better than that of current x-ray inelastic scattering techniques [4,8], to characterize the cubic-phase R-point scattering in MAPI. Data obtained from constant-$\mathbf{Q}$ scans (E scans), where energy transfer ($\hbar\omega$) is varied at a fixed momentum transfer $\mathbf{Q}$, and elastic $\mathbf{Q}$ scans,

where $\mathbf{Q}$ is varied at fixed $\hbar\omega = 0$, were compared to models representing dynamic-domain and *CP* hypotheses. The models are assessed in terms of line shape goodness of fit and temperature dependence of peak intensity and linewidth. We find that the *R*-point scattering is resolution limited in energy but not in $\mathbf{Q}$ and thus consistent with a manifestation of the *CP* phenomenon and not dynamic tetragonal domains. The wave-vector (momentum) dependence and weak temperature dependence of the *R*-point scattering is compared to theoretical predictions of the *CP* origin and differs distinctly from that reported in inorganic oxide- and fluoride-based perovskites.

Scattering at the cubic *R*-point $\mathbf{Q} = \frac{1}{2}(1\,3\,3)$ for a fully deuterated single crystal of $CD_3ND_3PbI_3$ (d_6-MAPI) was characterized using cold (SPINS) and thermal (BT4) neutron triple-axis spectrometers at the National Institute of Standards and Technology (NIST) Center for Neutron Research (NCNR). The d_6-MAPI crystal was oriented in the $(100)\perp(011)$ scattering plane as described previously [3]. A fully deuterated sample was used to reduce background from the large incoherent scattering cross-section of hydrogen. The MA^+ cation rotates nearly freely in the cubic phase, resulting in a quasielastic scattering (QES) contribution to the total *R*-point scattering that must be subtracted before further analysis [1,2]. Quasielastic scattering of this nature produces a signal that varies slowly with $\mathbf{Q}$, even with a fully deuterated sample, as deuterium, nitrogen, and iodine all exhibit small incoherent scattering cross-sections of 2, 0.5, and 0.3 barns, respectively.

Four different energy resolutions were obtained by varying the neutron final energy E_f and adjusting horizontal beam collimations. The energy and wave-vector resolution HWHM in each case were characterized as described in the Supplementary Material [34], which also contains Refs. [35–38]. The spectra were reduced and analyzed with the NIST NCNR DATA ANALYSIS AND VISUALIZATION ENVIRONMENT (DAVE) software package [39]. All fitted parameters are reported with errors of ± one standard deviation.

Figure 1(a) shows E scans measured at $\mathbf{Q} = \frac{1}{2}(1\,3\,3)$ and 340 K ($T_C + 12.5$ K) for all experimental configurations, scaled to the same peak intensity. The energy linewidths are resolution limited in each case. By contrast, wave-vector linewidths of elastic $\mathbf{Q}$ scans measured along [100] and [011] are not resolution limited (see Fig. S5 in the Supplemental Material [34]) and show little dependence on instrumental $\mathbf{Q}$ resolution.

To characterize the temperature dependence of the *R*-point scattering, E scans and elastic $\mathbf{Q}$ scans were measured at $\mathbf{Q} = \frac{1}{2}(1\,3\,3)$ on cooling from 340–327 K with an energy resolution of 0.095 meV ($E_f = 4$ meV). The best resolution of 0.065 meV HWHM ($E_f = 3.5$ meV) has reduced dynamic range and cannot cover the full *R*-point scattering profile. Figures 1(b) and 1(c) display E scans and $\mathbf{Q}$ scans measured along [100] at the indicated

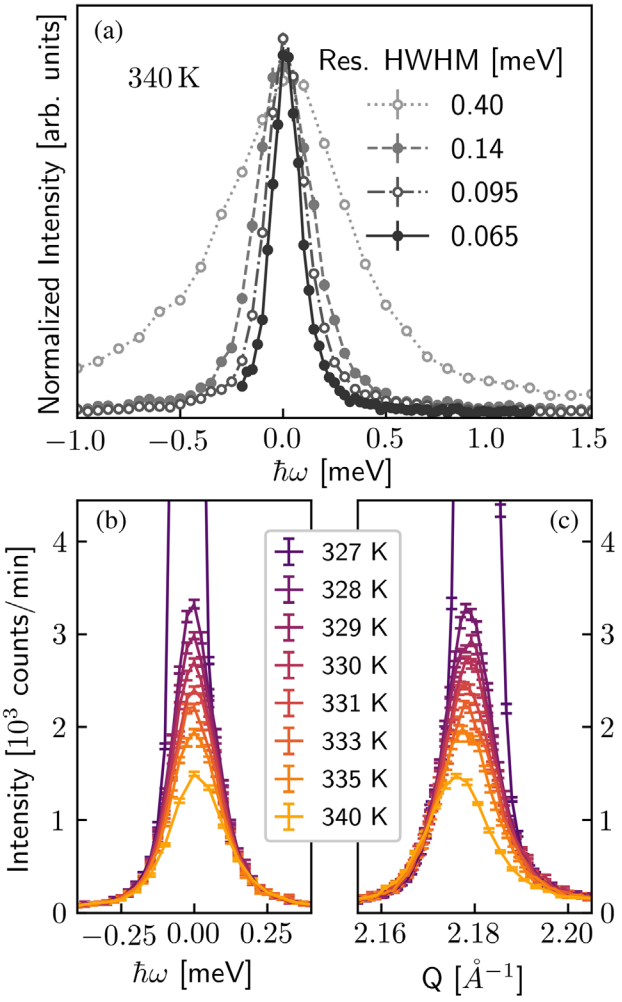

FIG. 1. Scattering at the cubic *R*-point $\mathbf{Q} = \frac{1}{2}(1\,3\,3)$ in d_6-MAPI measured with thermal and cold neutrons. In (a), the width of the scattering matches the energy resolution. Data were taken at 340 K on BT4 (dotted line) and SPINS (three other spectra). *R*-point scattering (b) energy and (c) wave-vector (at $\hbar\omega = 0$) dependence as a function of temperature measured with an energy resolution HWHM of 0.095 meV ($E_f = 4$ meV).

temperatures on SPINS. No phonon peaks are observed at any temperature in the *R*-point E scans up to $\hbar\omega = 4$ meV. This is not unexpected, as scattering from extremely short-lived phonons is indistinguishable from background at the zone boundary [3]. The scattering intensity increases slowly on cooling to 328 K but jumps at 327 K as the crystal undergoes a phase transformation. The cubic-tetragonal transition temperature T_C for d_6-MAPI is identified to be 327.5 ± 0.5 K, consistent with previous reports [40].

To obtain the QES contributions to the *R*-point scattering, we measured the scattering at $\mathbf{Q} = \frac{1}{2}(0.7\,3\,3)$ slightly offset from the *R* point at 330 K, as shown in Fig. 2(c). The QES was modeled with a delta function δ to capture the elastic incoherent scattering plus two Lorentzian functions $\mathcal{L}$ corresponding to fast methyl and ammonium group

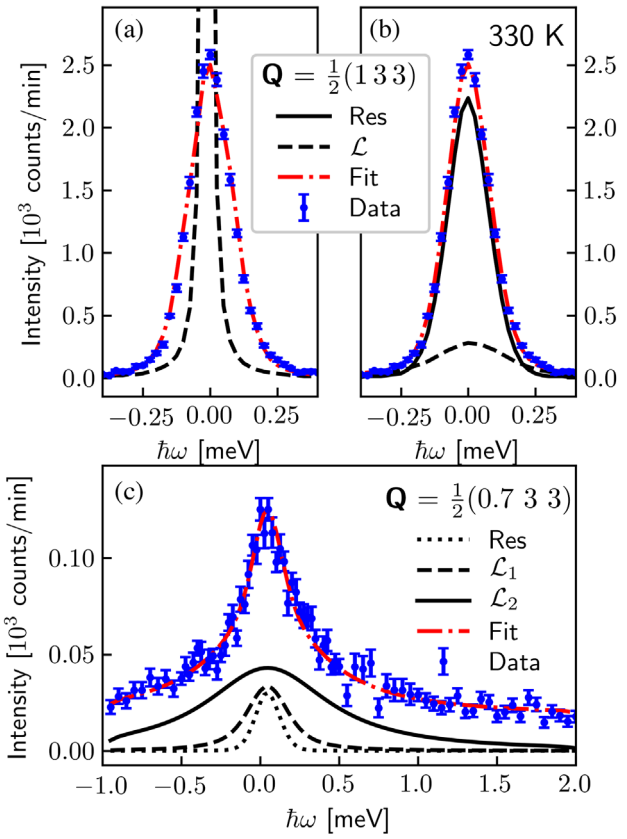

FIG. 2. Fits to the QES-subtracted R-point E scan (resolution HWHM = 0.095 meV) at 330 K using the (a) dynamic-domain (reduced-$\chi^2 = 3.41$) and (b) CP models (reduced-$\chi^2 = 1.42$). The resolution-broadened total fits are plotted as a red dash-dot line, the Lorentzian components $\mathcal{L}$ as black dashed lines, and the resolution-broadened delta function δ as a solid black line. The dynamic-domain model does not fit the tails or peak as well as the CP model. (c) Fit (dash-dot red line) of the QES offset from the R point to a model consisting of two $\mathcal{L}$ (dashed and solid black lines) and a δ function (dotted black line) convolved with the instrument resolution function plus a flat background (not shown).

rotations about the C–N bond axis and slower molecular reorientations perpendicular to this axis. Fitted linewidths yield mean residence times of 1.5 ps and 6.8 ps for fast and slow rotations, respectively, both within the range of reported values [1,2]. The QES scattering from $\mathbf{Q} = \frac{1}{2}(0.7\,3\,3)$ at 330 K was then subtracted from R-point scattering at all temperatures.

The dynamic-domain and CP hypotheses are tested by comparing results from fitting these models to the QES-subtracted R-point E scans. The dynamic-domain model consists of a single $\mathcal{L}$, whereas the CP model is the sum of a δ function (representing energy-resolution-limited scattering) and a $\mathcal{L}$ to account for remaining QES or other effects. Both models are convolved with the resolution function during the fit. Representative fits of these models to 330 K spectra are provided in Figs. 2(a) and 2(b). At all temperatures below 340 K (see Fig. S6 in the Supplemental Material [34]), the reduced-χ^2 statistic for the CP model is less than that of the dynamic-domain model, indicating the CP model better describes the data.

Within the dynamic-domain hypothesis, the lifetime τ of dynamic tetragonal domains is calculated from the HWHM of the $\mathcal{L}$ as $\tau = \hbar/\mathrm{HWHM}$ [41]. We determine a minimum τ for dynamic domains by constructing a highest posterior density interval (HPDI) from the log likelihood that R-point E scans are described by a resolution-broadened $\mathcal{L}$ of varying HWHMs. Details are provided in the Supplemental Material [34]. Minimum τ range from 17 ps to 47 ps at 340 K and 328 K, respectively. These results are plotted in Fig. 3(a) and show an unexpectedly weak dependence on temperature. The same analysis was performed for 340 K data with resolution HWHM = 0.065 meV, with a corresponding minimum $\tau = 36$ ps. These τ are an order of magnitude longer than both molecular rotation and zone-boundary phonon lifetimes [1–3].

Figure 2(b) demonstrates that under the CP model the scattering intensity is almost entirely described by the resolution function at 330 K. Figure 3(b) plots integrated intensity of the resolution-broadened δ component through T_C. Temperature-dependent area fractions of the δ and $\mathcal{L}$ components are plotted in Fig. S7 in the Supplemental Material [34]. Linewidths of the $\mathcal{L}$ component are converted to τ, which slowly decreases with temperature (see Fig. S8 in the Supplemental Material [34]).

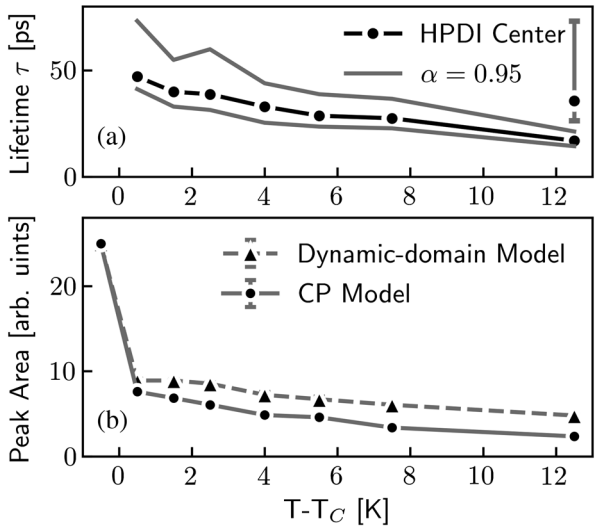

FIG. 3. (a) Minimum τ (and 95% confidence interval α) of tetragonal domains determined from maximum likelihood estimation. Temperature-dependent τ are determined from R-point E scans with resolution HWHM = 0.095 meV. The single point at $T - T_C = 12.5$ K corresponds to the R-point E scan with resolution HWHM = 0.065 meV. (b) Peak area obtained from R-point E scans, the CP model corresponds to the resolution-broadened δ component only. Error bars may be smaller than the corresponding marker.

To gain further insight into the two hypotheses, we analyze the momentum dependence of the R-point scattering. Elastic $\mathbf{Q}$ scans centered on $\frac{1}{2}(1\,3\,3)$ were measured along [100] on SPINS and along [100] and [011] on BT4. $\mathbf{Q}$ scans of critical scattering are expected to narrow toward the resolution limit as $T \to T_C$, whereas the CP is broader than the $\mathbf{Q}$ resolution HWHM at all temperatures [16,18]. The data at each temperature were fit with either a $\mathcal{L}$ or $\mathcal{L}^2$ function, convolved with the instrumental wave-vector resolution function, plus a flat background, as proposed by CP models [15,16,42,43]. The best line shape was determined by comparing reduced-χ^2 statistics. All scans measured on SPINS are best described by a $\mathcal{L}^2$ line shape. Figure 4(a) plots representative fits for SPINS spectra at 330 K; the $\mathcal{L}^2$ fit is significantly better than that for $\mathcal{L}$. Scans measured on BT4 (not shown) fit equally well to either line shape.

Linewidths extracted from $\mathcal{L}^2$ fits to elastic $\mathbf{Q}$ scans were converted to correlation lengths ξ using the relation $\xi = (\mathrm{HWHM}/0.64)^{-1}$ [16] and are plotted in Fig. 4(b). Correlation lengths range from 10–18 Å just above T_C with no significant anisotropy in $\mathbf{Q}$. These values are quite small, nearly an order of magnitude less than those measured in $RbCaF_3$ and $SrTiO_3$ at $(T - T_C) = 1$ K and 10 K, respectively [14,16,18]. The observed temperature dependence is very weak; any critical exponents extracted from inverse power law fits range from 0.07 to 0.17.

We now compare the two hypotheses in terms of the fitted parameters. The resolution-limited R-point E scans [Fig. 1(a)] are consistent with the CP phenomenon. It could be argued that a sufficiently narrow $\mathcal{L}$ convolved with a broad resolution function will also appear resolution limited [13]. In this case the tetragonal domain lifetime is at least 36 ps [Fig. 3(a)]. However, all other aspects of the R-point scattering are not consistent with this picture. First, the peak area, correlation length, and τ [Figs. 3(a), 3(b) and 4(b)] do not diverge near T_C, showing only weak temperature dependencies. Second, although the scattering is resolution limited in energy, it is not resolution limited in $\mathbf{Q}$. This behavior is hard to reconcile with critical scattering from dynamic domains but is fully consistent with the CP phenomenon [15,16]. Finally, the goodness of fit for the CP model is the better than the dynamic-domain model at all temperatures below 340 K.

Our analysis indicates that the R-point scattering observed in d_6-MAPI is a manifestation of the CP phenomenon. The remaining $\mathcal{L}$ component of the CP model is unlikely due to overdamped phonons or critical scattering because the linewidth is too narrow and the intensity and τ decrease on cooling to T_C [3] (see Figs. S7 and S8 in the Supplemental Material [34]). Given that it is a relatively small fraction of the total scattering, we believe it is more likely the result of an imperfect QES subtraction.

Resolution-limited scattering has been observed at the M and X points near phase transitions in $MAPbCl_3$ and

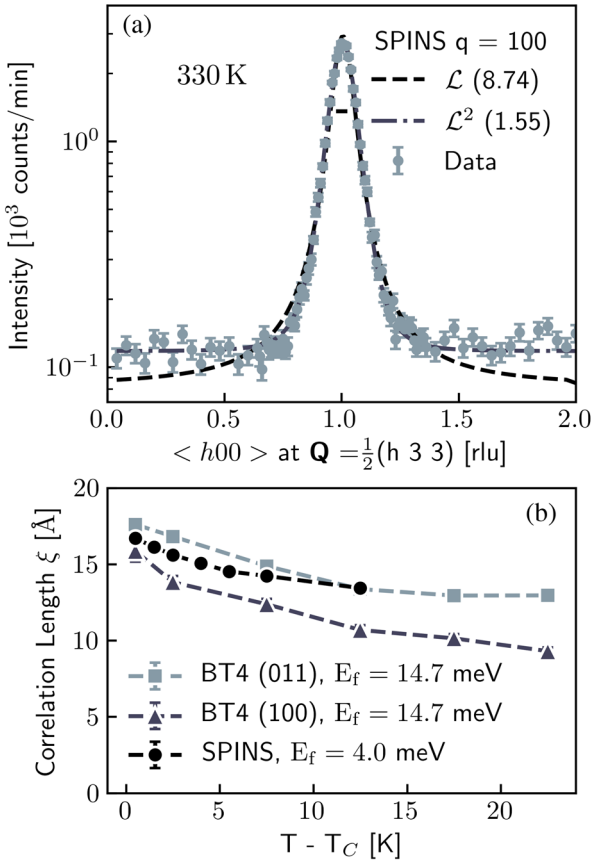

FIG. 4. (a) Representative elastic $\mathbf{Q}$ scan from SPINS at 330 K along [100] at the R point. The data (gray markers) are fit to both $\mathcal{L}$ (dashed) and $\mathcal{L}^2$ (dash-dot) line shapes, with corresponding reduced-χ^2 values indicated in the legend. Resolution FWHM is indicated with a black line. (b) Correlation lengths ξ extracted from $\mathcal{L}^2$ linewidths for R-point scans along [100] (SPINS, BT4) and [011].

$CsPbBr_3$, potentially indicating the existence of the CP in these materials as well [23,24]. By contrast, critical scattering with a dynamic component has been observed at the R point in $CsPbBr_3$ near the tetragonal-orthorhombic transition [24]. Off-centering due to lone pair stereochemistry and small domain formation are two dynamic processes proposed from x-ray PDF experiments [4,10,11]. No timescales can be derived because total scattering experiments are a static snapshot averaged over the probe size. Additionally, the off-centering effect is negligible in MAPI, and the length scale of the distortion is smaller than the ξ reported in Fig. 3(c) [11].

With the phonon-based CP origin, the line shape of the elastic $\mathbf{Q}$ scan depends on the renormalized mode frequency ω_0, quasiharmonic soft-mode frequency ω_∞, and a renormalization coupling constant $\delta^2 = \omega_\infty^2 - \omega_0^2$ [15,16]. When $\omega_\infty^2 \gg \delta^2$, the central peak is described by a $\mathcal{L}^2$ line shape; when $\omega_\infty^2 \approx \delta^2$, the line shape is $\mathcal{L}$. As the phonons are heavily damped near the zone boundary, we cannot measure ω_∞. However, the $\mathcal{L}^2$ line shape best describes all

elastic **Q** scans, suggesting that $\omega_0^2 > 0$ meV at all temperatures. This implies a first-order transition because ω_0 decreases toward zero for a second-order transition, as seen in $SrTiO_3$ [44,45]. In fact, the lattice parameter (see Fig. S12 in the Supplemental Material [34]) exhibits a discontinuous jump at T_C, thus confirming the cubic-tetragonal transition in d_6-MAPI is first order.

A $\mathcal{L}^2$ *CP* line shape can also arise from scattering by static domains of the low-temperature phase nucleating around isolated point defects [18,42,43,46]. In this picture, tetragonal domains in d_6-MAPI are 10–18 Å in diameter (2–3 unit cells). Nucleation may occur at iodide vacancies, which have extremely low formation energies of 0.08–0.22 eV and concentrations of 10^{17}–10^{20} cm^{-3} [47,48]. Furthermore, Imry and Wortis demonstrated that these defect-induced domains result in a smearing of a first-order phase transition about T_C [18,43,46]. The small domains, however, differ significantly from those in other perovskites, as scattering of this type is only observed from surface domains 1 to 2 orders of magnitude larger than the ξ in Fig. 4(b) [4,14,16,18,30,43]. Small ξ may result from weaker coupling between lead iodide octahedra, consistent with observations of extremely short acoustic phonon mean free paths near Brillouin zone boundaries and the fact that the lattice constant in MAPI (6.30 Å) is much larger than in conventional inorganic perovskites like $SrTiO_3$ (3.90 Å) [3].

The *CP* area and ξ do not diverge as $T \to T_C$ as is observed in $SrTiO_3$, $KMnF_3$, $RbCaF_3$, and $CsPbBr_3$ [14,18,24,28,49,50]. Critical exponents for these systems range from one to two for *CP* intensity and 0.5–0.84 for correlation lengths, both much larger than what we observe. In fact, the temperature dependence of the *CP* in d_6-MAPI above T_C is better described with a linear model. The lack of divergent behavior is further indication that the cubic-tetragonal phase transition in d_6-MAPI is first order.

In summary, we report neutron inelastic scattering experiments of d_6-MAPI through the cubic-tetragonal phase transition and find that the *CP* model provides a statistically better and more physically plausible description of the data. The *R*-point scattering is dominated by a resolution-limited signal, and the temperature dependence does not behave as expected for dynamical domains. We cannot determine the physical origin of the *CP* signal but propose that phonon coupling is not maintained with such extremely short phonon lifetimes at the zone boundary, thus the defect-based origin is more likely. The data we obtained set a lower bound on any dynamics of 36 ps at 340 K. We therefore conclude that the observed scattering is a manifestation of the *CP* phenomenon.

The authors acknowledge helpful discussions with Paul Kienzle regarding confidence intervals for lifetime estimation. This work (neutron scattering) was supported by the Center for Hybrid Organic Inorganic Semiconductors for Energy, an Energy Frontier Research Center funded by the Office of Basic Energy Sciences, an office of science within the US Department of Energy (DOE). H. I. K. acknowledges funding through the DOE Office of Basic Energy Sciences, Division of Materials Sciences and Engineering, under Contract No. DE-AC02-76SF0051. Any mention of commercial products here is for information only; it does not imply recommendation or endorsement by the National Institute of Standards and Technology.

*Corresponding author.
mftoney@slac.stanford.edu

[1] A. M. A. Leguy, J. M. Frost, A. P. McMahon, V. G. Sakai, W. Kockelmann, C. Law, X. Li, F. Foglia, A. Walsh, B. C. Oregan *et al.*, Nat. Commun. **6**, 7124 (2015).
[2] T. Chen, B. J. Foley, B. Ipek, M. Tyagi, J. R. D.Copley, C. M. Brown, J. J. Choi, and S.-H. Lee, Phys. Chem. Chem. Phys. **17**, 31278 (2015).
[3] A. Gold-Parker, P. M. Gehring, J. M. Skelton, I. C. Smith, D. Parshall, J. M. Frost, H. I. Karunadasa, A. Walsh, and M. F. Toney, Proc. Natl. Acad. Sci. U.S.A. **115**, 11905 (2018).
[4] A. N. Beecher, O. E. Semonin, J. M. Skelton, J. M. Frost, M. W. Terban, H. Zhai, A. Alatas, J. S. Owen, A. Walsh, and S. J. L. Billinge, ACS Energy Lett. **1**, 880 (2016).
[5] C. Quarti, E. Mosconi, J. M. Ball, V. D'Innocenzo, C. Tao, S. Pathak, H. J. Snaith, A. Petrozza, and F. D. Angelis, Energy Environ. Sci. **9**, 155 (2016).
[6] L. D. Whalley, J. M. Frost, Y.-K. Jung, and A. Walsh, J. Chem. Phys. **146**, 220901 (2017).
[7] M. T. Weller, O. J. Weber, P. F. Henry, A. M. D. Pumpo, and T. C. Hansen, Chem. Commun. (Cambridge) **51**, 4180 (2015).
[8] R. Comin, M. K. Crawford, A. H. Said, N. Herron, W. E. Guise, X. Wang, P. S. Whitfield, A. Jain, X. Gong, A. J. H. McGaughey *et al.*, Phys. Rev. B **94**, 094301 (2016).
[9] P. S. Whitfield, N. Herron, W. E. Guise, K. Page, Y. Q. Cheng, I. Milas, and M. K. Crawford, Sci. Rep. **6**, 35685 (2016).
[10] D. H. Fabini, G. Laurita, J. S. Bechtel, C. C. Stoumpos, H. A. Evans, A. G. Kontos, Y. S. Raptis, P. Falaras, A. Van der Ven, M. G. Kanatzidis *et al.*, J. Am. Chem. Soc. **138**, 11820 (2016).
[11] G. Laurita, D. H. Fabini, C. C. Stoumpos, M. G. Kanatzidis, and R. Seshadri, Chem. Sci. **8**, 5628 (2017).
[12] C. C. Stoumpos, C. D. Malliakas, and M. G. Kanatzidis, Inorg. Chem. **52**, 9019 (2013).
[13] W. G. Stirling and S. C. Perry, in *Introduction to Neutron Scattering* (PSI Proceedings, Switzerland, 1996), pp. 86–102.
[14] K. Hirota, J. P. Hill, S. M. Shapiro, G. Shirane, and Y. Fujii, Phys. Rev. B **52**, 13195 (1995).
[15] S. M. Shapiro, J. D. Axe, G. Shirane, and T. Riste, Phys. Rev. B **6**, 4332 (1972).
[16] G. Shirane, R. A. Cowley, M. Matsuda, and S. M. Shapiro, Phys. Rev. B **48**, 15595 (1993).
[17] U. J. Nicholls and R. A. Cowley, J. Phys. C **20**, 3417 (1987).
[18] T. W. Ryan, R. J. Nelmes, R. A. Cowley, and A. Gibaud, Phys. Rev. Lett. **56**, 2704 (1986).

[19] A. Gibaud, H. You, S. M. Shapiro, and J. Y. Gesland, Phys. Rev. B **42**, 8255 (1990).
[20] S. Ravy, D. Le Bolloch, R. Currat, A. Fluerasu, C. Mocuta, and B. Dkhil, Phys. Rev. Lett. **98**, 105501 (2007).
[21] M. Holt, M. Sutton, P. Zschack, H. Hong, and T.-C. Chiang, Phys. Rev. Lett. **98**, 065501 (2007).
[22] Y. Fujii, S. Hoshino, Y. Yamada, and G. Shirane, Phys. Rev. B **9**, 4549 (1974).
[23] M. Songvilay, M. Bari, Z.-G. Ye, G. Xu, P. M. Gehring, W. D. Ratcliff, K. Schmalzl, F. Bourdarot, B. Roessli, and C. Stock, Phys. Rev. Mater. **2**, 123601 (2018).
[24] M. Songvilay, N. Giles-Donovan, M. Bari, Z.-G. Ye, J. L. Minns, M. A. Green, G. Xu, P. M. Gehring, K. Schmalzl, W. D. Ratcliff *et al.*, Phys. Rev. Mater. **3**, 093602 (2019).
[25] C. Stock, M. Songvilay, P. M. Gehring, G. Xu, and B. Roessli, J. Phys. Condens. Matter **32**, 374012 (2020).
[26] T. Riste, E. J. Samuelsen, K. Otnes, and J. Feder, Solid State Commun. **9**, 1455 (1971).
[27] R. A. Cowley, Phys. Scr. T **T66**, 24 (1996).
[28] J. B. Hastings, S. M. Shapiro, and B. C. Frazer, Phys. Rev. Lett. **40**, 237 (1978).
[29] A. Gibaud, T. W. Ryan, and R. J. Nelmes, J. Phys. C **20**, 3833 (1987).
[30] D. F. McMorrow, N. Hamaya, S. Shimomura, Y. Fujii, S. Kishimoto, and H. Iwasaki, Solid State Commun. **76**, 443 (1990).
[31] H.-B. Neumann, U. Rütt, J. R. Schneider, and G. Shirane, Phys. Rev. B **52**, 3981 (1995).
[32] P. M. Gehring, K. Hirota, C. F. Majkrzak, and G. Shirane, Phys. Rev. B **51**, 3234 (1995).
[33] H. Hünnefeld, T. Niemöller, J. R. Schneider, U. Rütt, S. Rodewald, J. Fleig, and G. Shirane, Phys. Rev. B **66**, 014113 (2002).
[34] See Supplemental Material at http://link.aps.org/supplemental/10.1103/PhysRevLett.125.075701 for additional experimental details, discussion of the resolution function, and details of the statistical analysis of domain lifetimes.
[35] G. Shirane, S. M. Shapiro, and J. M. Tranquada, *Neutron Scattering with a Triple-Axis Spectrometer: Basic Techniques* (Cambridge University Press, Cambridge, United Kingdom, 2002).
[36] E. Farhi, Y. Debab, and P. Willendrup, J. Neutron Res. **17**, 5 (2014).
[37] M. Newville, R. Otten, A. Nelson, A. Ingargiola, T. Stensitzki, D. Allan, A. Fox, F. Carter, Micha, D. Pustakhod *et al.*, lmfit/lmfit-py 1.0.0 (2019) https://doi.org/10.5281/zenodo.3588521.
[38] Y. Kawamura, H. Mashiyama, and K. Hasebe, J. Phys. Soc. Jpn. **71**, 1694 (2002).
[39] R. T. Azuah, L. R. Kneller, Y. Qiu, P. Tregenna-Piggott, C. M. Brown, J. R. D. Copley, and R. M. Dimeo, J. Res. Natl. Inst. Stand. Technol. **114**, 341 (2009).
[40] A. Poglitsch and D. Weber, J. Chem. Phys. **87**, 6373 (1987).
[41] A. A. Maradudin and A. E. Fein, Phys. Rev. **128**, 2589 (1962).
[42] B. I. Halperin and C. M. Varma, Phys. Rev. B **14**, 4030 (1976).
[43] A. Gibaud, R. A. Cowley, and P. W. Mitchell, J. Phys. C **20**, 3849 (1987).
[44] C. A. Occhialini, G. G. Guzmán-Verri, S. U. Handunkanda, and J. N. Hancock, Front. Chem. Proc. Front. Chem. Conf. **6**, 545 (2018).
[45] J. F. Scott, Rev. Mod. Phys. **46**, 83 (1974).
[46] Y. Imry and M. Wortis, Phys. Rev. B **19**, 3580 (1979).
[47] A. Walsh, D. O. Scanlon, S. Chen, X. G. Gong, and S.-H. Wei, Angew. Chem., Int. Ed. Engl. **54**, 1791 (2015).
[48] G. Richardson, S. E. J. O'Kane, R. G. Niemann, T. A. Peltola, J. M. Foster, P. J. Cameron, and A. B. Walker, Energy Environ. Sci. **9**, 1476 (2016).
[49] U. J. Cox, J. Phys. Condens. Matter **1**, 3565 (1989).
[50] U. J. Cox and L. D. Cussen, J. Phys. Condens. Matter **1**, 3579 (1989).